

Oil & Natural Gas Technology

DOE Award No.: DE-FE0009897

Quarterly Research Performance Progress Report (Period ending 12/31/2014)

Hydrate-Bearing Clayey Sediments: Morphology, Physical Properties, Production and Engineering/Geological Implications

Project Period (10/1/2012 to 9/30/2016)

Submitted by:
J. Carlos Santamarina



Georgia Institute of Technology
DUNS #: 097394084
505 10th street
Atlanta , GA 30332
e-mail: jcs@gatech.edu
Phone number: (404) 894-7605

Prepared for:
United States Department of Energy
National Energy Technology Laboratory

Submission date: 1/31/2014



Office of Fossil Energy

DISCLAIMER:

This report was prepared as an account of work sponsored by an agency of the United States Government. Neither the United States Government nor any agency thereof, nor any of their employees, makes any warranty, express or implied, or assumes any legal liability or responsibility for the accuracy, completeness, or usefulness of any information, apparatus, product, or process disclosed, or represents that its use would not infringe privately owned rights. Reference herein to any specific commercial product, process, or service by trade name, trademark, manufacturer, or otherwise does not necessarily constitute or imply its endorsement, recommendation, or favoring by the United States Government or any agency thereof. The views and opinions of authors expressed herein do not necessarily state or reflect those of the United States Government or any agency thereof.

ACCOMPLISHMENTS

Context – Goals. *Fine grained sediments host more than 90% of the global gas hydrate accumulations. Yet, hydrate formation in clayey sediments is least understood and characterized. This research focuses on hydrate bearing clayey sediments. The goals of this research are (1) to gain a fundamental understanding of hydrate formation and ensuing morphology, (2) to develop laboratory techniques to emulate “natural” formations, (3) to assess and develop analytical tools to predict physical properties, (4) to evaluate engineering and geological implications, and (5) to advance gas production alternatives to recover methane from these sediments.*

Accomplished

The main accomplishments for this period include:

- Formation of CO₂ hydrate in fine-grained sediment with segregated topology
- Numerical solution for material properties
- Studies of production and implications

Plan - Next reporting period

Further develops in laboratory specimens, physical properties, and gas production. This report centers on the well-sediment interaction during gas production.

Research in Progress: Well-Sediment Interaction During Production

Gas hydrate is found in marine sediments and within the permafrost. Hydrate formation requires the presence of gas and water, and a combination of high pressure and low temperature conditions that falls within the stability field. High water pressures u_o imply deep water columns (typical water pressures are in excess of 10-to-20 MPa). On the other hand, the low temperature requirement combines with the natural geothermal gradient to limit hydrate accumulation in shallow sediments beneath the seafloor; hence, hydrate bearing sediments are subjected to low in-situ effective stress σ'_o (Figure 1a).

Gas can be recovered from hydrate bearing sediments by depressurization, heating, chemical-driven dissociation (by shifting the phase boundary), and molecular exchange (e.g., $\text{CO}_2\text{-CH}_4$). Depressurization appears to be the most viable alternative in most cases. A pronounced decrease in pore fluid pressure Δu_o is needed to cause dissociation and to extend the dissociation front to a considerably distance r^* away from the borehole (Figure 1b). A decrease in pore fluid pressure implies an increase in effective stress $\Delta\sigma'$. In fact, it follows from the previous observations that the change in effective stress $\Delta\sigma'$ during depressurization-driven gas production can largely exceed the initial effective stress in situ σ'_o , that is $\Delta\sigma' \gg \sigma'_o$. Then, the following changes are anticipated during depressurization-driven gas production: large volume compaction, marked increase in stiffness, pronounced decrease in hydraulic conductivity, and an increase in thermal conductivity (albeit diminished by the decreased water saturation). These changes are coupled and vary throughout the affected volume.

Sediment compaction in and around the production horizon challenges the engineering design of production wells. The sediment-well interaction is a classical soil-structure interaction problem in geomechanics, similar to pile foundation analysis but with a few important caveats and differences. First, the axial load imposed at the top of the well may be null, yet, the well can be intensely loaded by the negative skin friction mobilized as the sediment contracts at depth during the depressurization of the hydrate bearing layer. Second, the high increase in effective stress near the well alters the sediment response. In contrast, piles are loaded at the top and the sediment is intimately related to initial conditions before the installation of the pile.

Careful analysis is required to anticipate the consequences of depressurization and to properly engineer the well installation/termination and production strategy. The study documented herein

focuses on the governing variables and conditions that determine the geomechanical well-sediment interaction, explores unanticipated emergent phenomena, and suggests alternatives for bottom hole termination. The study focuses on the hydro-mechanical coupled sediment-well interaction problem and does not take into consideration the chemo-thermal effects associated to hydrate dissociation. First, the sediment-well interaction problem is explored using a simplified, yet insightful analysis. Then, a comprehensive finite element model is used to explore the fully coupled hydro-mechanical problem to reveal the full consequences of depressurization.

Models and Constitutive Equations

We document first new constitutive equations developed to model large stress changes, the selection of boundary conditions, and the modeling of the production well.

Sediment volume compaction. Soft marine sediments subjected to low initial effective stress σ'_o experience pronounced volume contraction when subjected to high effective stress changes $\Delta\sigma'$ during depressurization where typically $\Delta\sigma' \gg \sigma'_o$. The classical Terzaghi-type void-ratio-stress compressibility curve is modified to avoid unrealistically high void ratios near the seafloor or negative void ratios near the wall during depressurization

$$e = e_{1\text{kPa}} - C_c \log\left(\frac{1\text{kPa}}{\sigma' + \sigma'_L} + \frac{1\text{kPa}}{\sigma'_H}\right)^{-1} \quad (1)$$

The low and high stress constants σ'_L and σ'_H are selected such that the asymptotic low and high asymptotic void ratios e_L and e_H are

$$e_L = e_{1\text{kPa}} - C_c \log\left(\frac{\sigma'_L}{1\text{kPa}}\right) \quad (2)$$

$$e_H = e_{1\text{kPa}} - C_c \log\left(\frac{\sigma'_H}{1\text{kPa}}\right) \quad (3)$$

Sediment hydraulic conductivity. Various sediment parameters change with effective stress and/or void ratio. For the purposes of this hydro-mechanical coupled study, the evolution of hydraulic conductivity k [cm/s] is most relevant and is modeled as a function of void ratio e

$$\frac{k}{k_o} = \left(\frac{e}{e_o} \right)^b \quad (4)$$

where k_o [cm/s] is the hydraulic conductivity at the reference void ratio e_o , and the b -exponent captures the sensitivity of hydraulic conductivity to changes in void ratio. For fine grained sediments the exponent can be $b=4$ and larger.

Sediment-well interface. Elasto-plastic and hyperbolic models are selected to capture the load versus the relative shear displacement between the sediment and the well. In both cases, the ultimate shear strength of the interface is proportional to the normal effective stress in the radial direction σ'_r and the sediment-well friction angle ϕ (Coulomb model),

$$\tau_{ult} = \sigma'_r \tan \phi \quad (5)$$

The interface shear stiffness k_s increases as the normal effective stress increases. We capture this response by making k_s proportional to τ_{ult} through a threshold sediment-wall shear displacement δ^*

$$k_s = \frac{\tau_{ult}}{\delta^*} \quad (6)$$

The bilinear elasto-plastic model is fully defined by k_s , δ^* and τ_{ult} . The hyperbolic model is computed as

$$\tau = \frac{\delta}{\delta^* + |\delta|} \tau_{ult} \quad (7)$$

The threshold deformation is related to the well diameter D_{well} in lumped element models, e.g., $\delta^* \approx D_{well}/20$ in part to take into account near-field sediment deformation; instead, finite element codes use proper shear response data. When $\delta = \delta^*$, the elasto-plastic model predicts $\tau = \tau_{ult}$ while the hyperbolic model shows $\tau = \tau_{ult}/2$. Consequently, lower threshold values δ^* are selected for the hyperbolic model in order to obtain results that are similar to those predicted with the elasto-plastic formulations.

Lumped Elements Model - Simplified Analysis

Equilibrium analysis results in the following differential equation that relates the axial force along the well P_z at depth z with the mobilized shaft resistance τ_z at depth z ,

$$\frac{\partial P_z}{\partial z} dz = -\pi D_{\text{well}} \tau_z dz \quad (8)$$

In finite differences

$$P_z^i - P_z^{i+1} = -(\pi D_{\text{well}} \Delta z) \tau_z^i \quad (9)$$

Finite Element Model – Fully Coupled 3D Analysis

All finite element simulations are fully coupled hydro-mechanical conditions, where the sediment is represented with a Cam Clay material model, but with compressibility described by Equation 1, and the associated hydraulic conductivity satisfies Equation 4. The formation is first subjected to zero-lateral strain self-weight gravitational loading (normally consolidated NC condition). Then, the medium is subjected to localized pore fluid depressurization. The axi-symmetric geometry has the following boundary conditions:

- top surface: zero vertical effective stress and constant fluid pressure
- Well: elastic shell elements
- Well-wall interface: thin surface elements with elasto-plastic response (Equation 5)
- Base and Far-field radial boundary: zero normal strain, zero frictional resistance, and constant fluid pressure.

Preliminary studies conducted using a poroelastic medium showed marked effects of the far-field lower and radial boundaries. Boundaries were gradually placed further away until all boundary biases vanished.

Well. The well is modelled as an elastic pipe with a closed bottom at the tip. There is an internal isolation plate that separates the production zone from the upper part of the well. The pipe, the bottom plate and the isolation plate are represented using conical shell elements. Above the isolation plate, the well is subjected to internal hydrostatic pressure $u_0(z)$. Below the isolation plate, the internal fluid pressure evolves with the fluid pressure history that is imposed on the sediment.

The internal fluid pressure acts against all “steel faces”, i.e., the pipe, upper and lower faces of the isolation plate, and the bottom plate. Thin interface elements are used to model the sediment-well interface; these interface elements have an elasto-plastic response as described in Equations 5 and 6.

Initial conditions. Gravitational initial conditions are adopted for the simulations. Therefore, the sediment is subjected to self-weight consolidation; the sediment unit weight satisfies Equation 1 at all depths. We assume that the well installation does not change the in-situ state of stress and there is no residual shear between the well and the formation after installation.

Depressurization. Production by depressurization Δu is simulated by reducing the fluid pressure in the first layer of elements next to the well along the production zone from the initial hydrostatic condition u_0 to a value $u_0 - \Delta u$. For equilibrium, the internal pressure imposed onto steel faces inside the well is reduced by the same amount Δu beneath the isolation plate; above the isolation plate, the internal hydrostatic pressure imposed onto steel faces inside the well remains at the initial values before production $u_0(z)$.

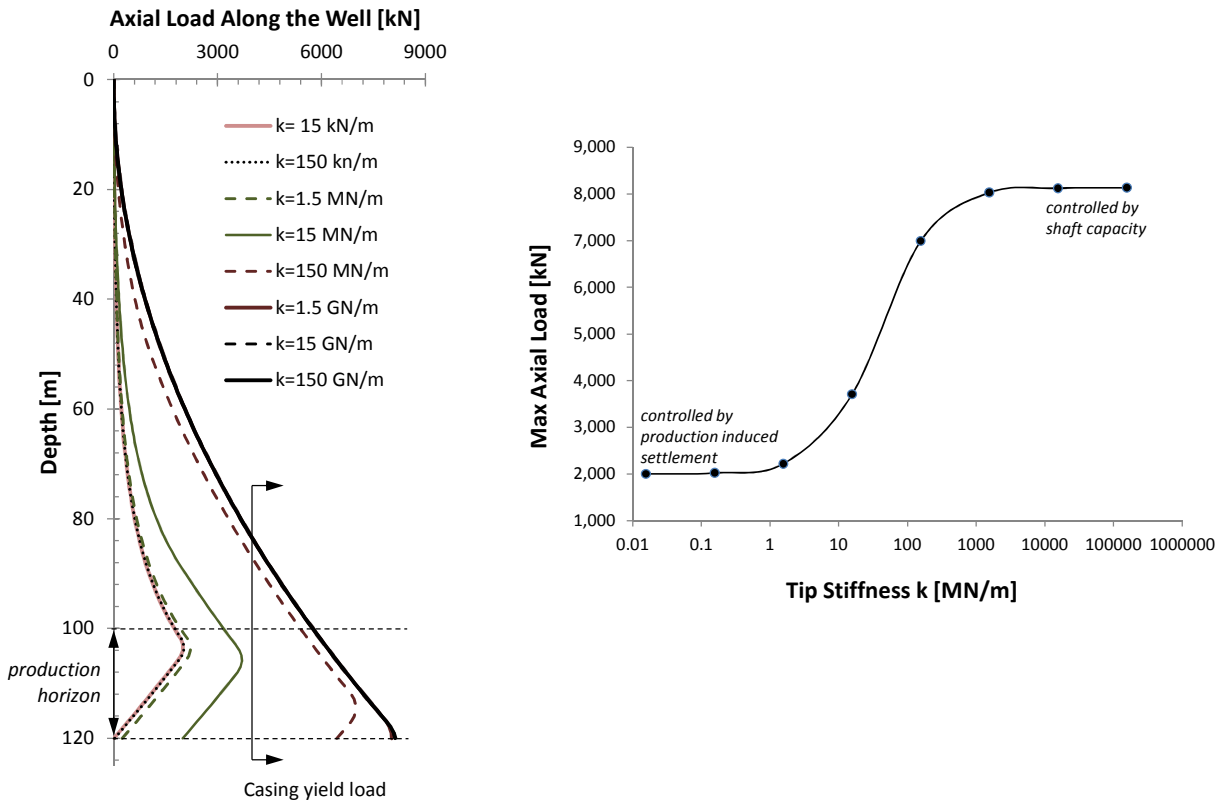
Numerical Model Verification. The code was verified against analytically tractable cases, including: self-weight consolidation under 1D conditions, radial flow (perfectly rigid porous medium of constant permeability), and well-sediment interaction (as a loaded perfectly rigid pile foundation in an elasto-plastic medium – with and without tip resistance). In all cases, solutions were in full agreement with numerical predictions.

Numerical Results

Geometry. The simulated field case represents conditions relevant to various hydrate bearing formations that could be considered for production: 2000m deep water column, and 170m deep well. A depressurization of $\Delta = -6\text{MPa}$ is imposed along the 15m long production screen between 150-and-165 mbsf. Four sediments are considered for this study. A subset of results is presented in this report, with emphasis on the high plasticity soft sediment.

Lumped parameter results. Figure 1 shows the axial load with depth for various values of the tip stiffness. Positive shaft resistance is mobilized within and below the production horizon, however, negative shaft resistance or down-drag takes place all along the sediment column above the

depressurization depth. The maximum load on the well may reach the elastic limit, particularly if high tip resistance develops (e.g., strong stratum below the production horizon). The maximum axial load varies between two extreme conditions determined either by the tip resistance/stiffness (“bottom sink”) and the maximum shaft capacity that can be mobilized in the overlying sediments (“shaft failure”).



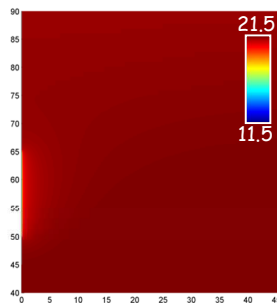
Finite element results. The coupled hydro-mechanical response leads to similar axial load distributions for similar conditions. However, the fully coupled formulation reveals pore pressure and deformation fields quite distinct from those hypothesized for the simpler analyses. In particular (see figures):

- The sediment does experience very high volumetric contraction as anticipated (Table 1). However, most of the volumetric deformation takes place in the radial direction. Hence, the

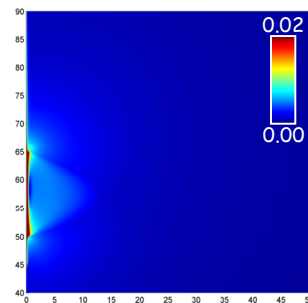
vertical settlement in the production horizon is an order of magnitude smaller than expected from simplified analyses.

- The vertical settlement is sufficient to mobilize the shaft resistance along the production well, hence there is clear similarity between the load distribution obtained with the lumped parameter formulation and results produced by the coupled hydro-mechanical finite element model.
- The intense modification the sediment experiences around the well in the production horizon shields the potential effects of tip conditions. Hence, more complex well termination conditions, such as compressible/telescopic tips appear unjustified at this point. The engineering of well termination requires further analyses.

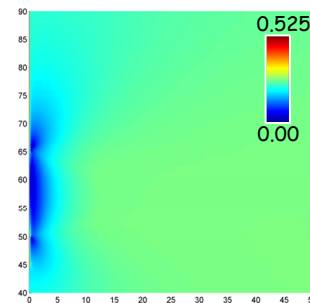
PWP [Mpa]



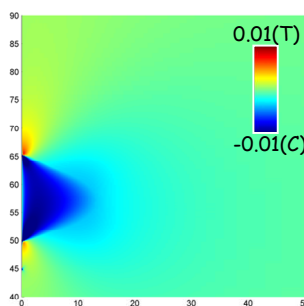
ϵ_q



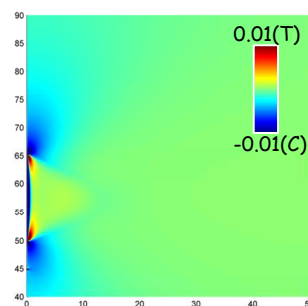
q/p



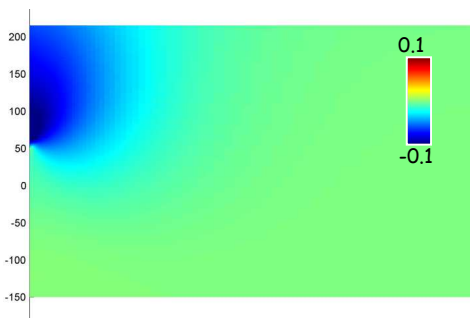
Vertical strain



Horizontal strain



Vertical settlement [m]



Discussion - Implications

Early tensile stress in the well above the production horizon. The formation of a localized compression bulb around the well in the production horizon during early production stages (i.e., during pressure diffusion and before steady state seepage) may trigger soil arching in the upper lay-

ers and cause tension in the production well. Tension does not appear to be sufficient to cause the tensile failure of a continuous well, but may cause joint/connector slippage.

Highly compressed zone around the well. The pronounced increase in effective stress associated with the high depressurization required for gas production has pronounced implications on the engineering of production systems and the extent of gas production. The coupled processes include: depressurization → increased effective stress → sediment compaction → reduced hydraulic conductivity → altered pressure field.

Reduced production zone. The combination of these couplings with radial flow conditions result in a fast recovery of the pressure field and a reduced radial distance to the end of the production zone, i.e., where the pressure recovers to values inside stability conditions.

Preliminary Conclusions

This study explored the geomechanical implications of depressurization, with emphasis on well-formation interaction. The analysis is particularly pertinent to gas production from hydrate bearing sediments (however, hydrate dissociation is not modelled and emphasis is placed on steady state conditions). Results show:

- High compressive forces develop in the well. The peak is typically found within the production horizon. These forces may cause yield and well collapse. Lower and upper bound estimates can be readily computed.
- A transient tension force may develop in the well above the production horizon.
- Adequate constitutive models are needed to capture soil compaction and the evolution of hydraulic conductivity during compaction.
- Hydraulic conductivity can decrease very dramatically near the well. This has profound implications to the development of the pressure field, effective stresses and compaction away from the well.
- In particular, the higher the sensitivity of hydraulic conductivity to compaction, the narrower the production zone becomes. Results show a pronounced decrease in the production zone even in sandy deposits.

MILESTONE LOG

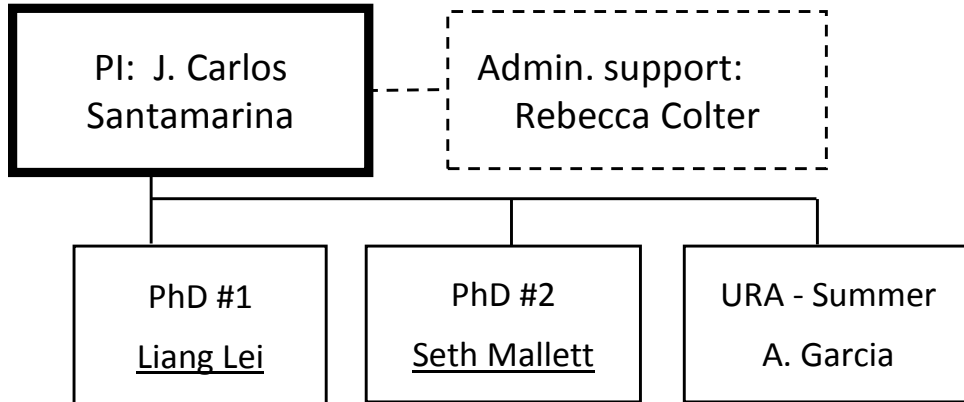
Milestone	Planned completion date	Actual completion date	Verification method	Comments
Literature review	5/2013	5/2013	Report	Completed first phase. Will continue throughout the project
Preliminary laboratory protocol	8/2013	8/2013	Report (with preliminary validation data)	this and previous reports
Cells for Micro-CT	8/2013	8/2013	Report (with first images)	this and previous reports
Compilation of CT images: segregated hydrate in clayey sediments	8/2014	Completed Additional tests in progress	Reports (with images)	Given the complexity of hydrate formation in clays, this task continues to explore additional conditions
Preliminary experimental studies on gas production	12/2014	Completed. Additional tests in progress	Report (with images)	
Analytical/numerical study of 2-media physical properties	5/2015	In progress	Report (with analytical and numerical data)	
Experimental studies on gas production	12/2015		Report (with data)	
Early numerical results related to gas production	5/2016	In progress	This report	
Comprehensive results (includes Implications)	9/2016		Comprehensive Report	

PRODUCTS

- **Publications:**
In progress
- **Presentations:**
In progress
- **Website:** Publications and key presentations are included in <http://pmrl.ce.gatech.edu/> (for academic purposes only)
- **Technologies or techniques:** X-ray tomographer and X-ray transparent pressure vessel
- **Inventions, patent applications, and/or licenses:** None at this point.
- **Other products:** None at this point.

PARTICIPANTS & OTHER COLLABORATING ORGANIZATIONS

Research Team: The current team is shown next. We anticipate including external collaborators as the project advances



IMPACT

While it is still too early to assess impact, we can already highlight preliminary success of exploring hydrate lenses morphology in real systems, and analogue studies using a high resolution tomographer.

CHANGES/PROBLEMS:

None at this point.

SPECIAL REPORTING REQUIREMENTS:

We are progressing towards all goals for this project.

BUDGETARY INFORMATION:

As of the end of this research period, expenditures are summarized in the following table.

Note: in our academic cycle, higher expenditures typically take place during the summer quarter.

Baseline Reporting Quarter DE-FE009897	Budget Period 1								Budget Period 2									
	Q1		Q2		Q3		Q4		Q1		Q2		Q3		Q4		Q1	
	10/1/12 - 12/31/12		1/1/13 - 3/31/13		4/1/13 - 6/30/13		7/1/13 - 9/30/13		10/1/13 - 12/31/13		1/1/14 - 3/31/14		4/1/14 - 6/30/14		7/1/14 - 9/30/14		10/1/14 - 12/31/14	
	Q1	Cumulative Total	Q2	Cumulative Total	Q3	Cumulative Total	Q4	Cumulative Total	Q1	Cumulative Total	Q2	Cumulative Total	Q3	Cumulative Total	Q4	Cumulative Total	Q1	Cumulative Total
Baseline Cost Plan																		
Federal Share	36,664	36,664	36,664	73,327	36,664	109,991	36,664	146,654	38,578	185,232	38,578	223,811	38,578	262,389	38,578	300,967	40,059	341,026
Non-Federal Share	10,922	10,922	10,922	21,844	10,922	32,765	10,922	43,687	11,250	54,937	11,250	66,186	11,250	77,436	11,250	88,685	11,587	100,272
Total Planned	47,585	47,585	47,585	95,171	47,585	142,756	47,585	190,341	49,828	240,169	49,828	289,997	49,828	339,824	49,828	389,652	51,647	441,299
Actual Incurred Cost																		
Federal Share	0	0	16,173	16,173	20,191	36,364	66,556	102,920	22,923	125,843	16,448	142,290	89,396	231,686	43,595	275,281	57,809	333,090
Non-Federal Share	0	0	52,426	52,426	13,106	65,532	0	65,532	28,443	93,975	28,443	122,418	-45,818	76,600	-1,866	74,735	25,961	100,696
Total Incurred Costs			68,600	68,600	33,297	101,897	66,556	168,453	51,366	219,818	44,891	264,709	43,578	308,287	41,729	350,016	83,770	433,786
Variance																		
Federal Share	-36,664	-36,664	-20,490	-57,154	-16,473	-73,626	29,893	-43,734	-15,656	-59,389	-22,131	-81,520	50,818	-30,702	5,017	-25,686	17,749	-7,936
Non-Federal Share	-10,922	-10,922	41,505	30,583	2,184	32,767	-10,922	21,845	17,194	39,039	17,194	56,232	-57,068	-835	-13,115	-13,950	14,374	424
Total Variance	-47,585	-47,585	21,015	-26,571	-14,289	-40,859	18,971	-21,888	1,538	-20,351	-4,937	-25,288	-6,250	-31,537	-8,098	-39,636	32,123	-7,512

National Energy Technology Laboratory

626 Cochrans Mill Road
P.O. Box 10940
Pittsburgh, PA 15236-0940

3610 Collins Ferry Road
P.O. Box 880
Morgantown, WV 26507-0880

13131 Dairy Ashford Road, Suite 225
Sugar Land, TX 77478

1450 Queen Avenue SW
Albany, OR 97321-2198

Arctic Energy Office
420 L Street, Suite 305
Anchorage, AK 99501

Visit the NETL website at:
www.netl.doe.gov

Customer Service Line:
1-800-553-7681

